A novel 4-DOF wide-range tunable frequency selective surface using an origami "eggbox" structure

Yepu Cui [ID], Ryan Bahr, Samantha Van Rijs and Manos Tentzeris

Georgia Institute of Technology, 85 5th St NW, Atlanta, GA 30308, USA

Abstract

Shape-changing mechanical metamaterials have drawn the attention of researchers toward the development of continuous-range tunable frequency selective surfaces (FSSs). In this paper, a novel tunable FSS utilizing an origami-inspired "eggbox" structure is presented featuring four-degrees of freedom that can change the frequency response of two orthogonal linear polarizations. The centrosymmetric "eggbox" structure can be folded or rotated along two axes that lead to unprecedented reconfigurability compared to traditional Miura-Ori-based structures which have fewer degrees of control. The utilized cross-shaped dipole FSS element shows enhanced bandwidth, support for orthogonal linear polarization, and ease of fabrication. The prototype is fabricated using a low-cost fully additive inkjet printing process with silver nanoparticle conductive ink. The outcome of this study shows a 25% frequency tunable range over two polarization directions. The design can be an ideal spatial filtering candidate for advanced ultra-wideband terrestrial and space applications.

CAMBRIDGE
UNIVERSITY PRESS

Introduction

A frequency selective surface (FSS) is a periodic structure with arrays of elements arranged on a dielectric substrate to absorb, reflect, or transmit electromagnetic waves based on the frequency [1]. The frequency response of an FSS can be determined by the element shape, size, distribution, and the type of the dielectric substrate. FSSs have found great range of applications including spatial frequency filtering [2], electromagnetic shielding [3], absorbers [4], radomes [5], sensors [6], etc.

In recent years, a significant amount of research has been undertaken on reconfigurable FSSs to realize a variable frequency response. Various methodologies can be utilized to achieve on-demand tunability, with one common approach is by introducing active components such as p–i–n diodes [7], varactor diodes [8, 9], or microelectromechanical systems (MEMS) capacitors/switches [10] to tune the parameters of the FSS equivalent circuits. The active tuning approach can be responsive and accurate. However, those active components can be expensive, fragile, and require complex biasing circuits that dramatically increase the cost and fabrication difficulty, limiting the scalability of the reconfigurable FSS.

Another approach to realize reconfigurable FSSs is by tuning the geometry mechanically using foldable origami-based 3D structures. A great number of origami-inspired 3D FSSs have been studied in recent years [2, 4, 11–14], showing unprecedented capabilities for deployability and continuous-range on-demand tunability. Miura-Ori [15, 16] is one of the most commonly used element structures in origami-inspired 3D FSS designs. A Miura-Ori FSS (M-FSS) features tunable equivalent electrical length and inter-element coupling by compressing from one side or changing the angle of incidence (AoI). Although compressing an M-FSS enables precise positioning by maintaining constant interspacing of elements along that axis, but it also removes a degree of freedom in the tuning parameters of an FSS device. Thus, the tunable range can be limited and insufficient in advanced ultra-wideband terrestrial and outer-space applications.

In this paper, a novel tunable origami-inspired 3D FSS is presented using an "eggbox" structure. The "eggbox" FSS can be tuned by compressing from two directions, or rotating from two axes. The multiple tuning methods enable a wider frequency tuning range. The prototype was fabricated with inkjet printing technique that is scalable, low-cost, and fully additive. The measured sample shows wide-range frequency tunability, four-degrees of freedom (4-DOF) and two orthogonal linear polarizations. This paper is an extended version of [17]; the extended content includes: mathematical analysis of the "eggbox" model; 4-DOF tuning method by folding β and α, rotating x-axis and y-axis; extended folding angle measurement result to get more accurate fractional bandwidth.
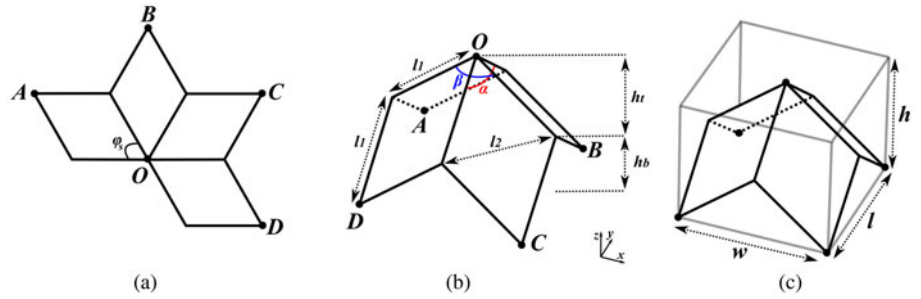
Fig. 1. Eggbox element design: (a) 2D flat eggbox outline pattern; (b) 3D-folded eggbox structure; and (c) 3D-folded eggbox volumetric boundary box.
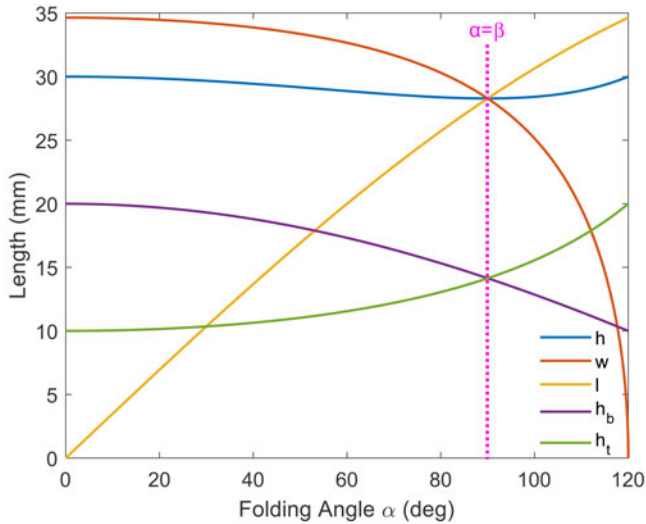
(a) (b) (c)

Fig. 2. Variation of different geometric parameters with folding angles α from 0 to 120°.
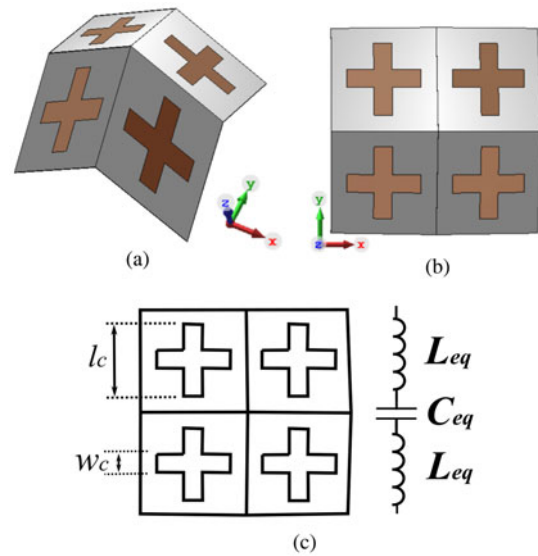

Fig. 3. Design of cross-dipole eggbox FSS element: (a) perspective view; (b) top view; and (c) equivalent circuit.

Element design

Mechanical design

The "eggbox" is a non-developable structure which features additional degrees of freedom compared to widely used Miura-Ori structure [18–20]. The design of an eggbox element is shown in Fig. 1(b). The bi-directional symmetry nature of the eggbox enables the ability to compress the eggbox structure from two orthogonal directions, in this case, x-axis and y-axis. The size of the eggbox is defined by two lengths l_1 and l_2. The compressing angles along the y-axis and x-axis are defined by α and β. When the eggbox is not compressed, α and β will be equal, which can be calculated by using (1):

$$\alpha = \beta = \theta_0 = 2 \times \arccos\left(\sqrt{\left(1 - \frac{l_2^2}{2l_1^2}\right)}\right) \qquad (1)$$

When the eggbox is compressed, the relation between the two folding angles α and β can be calculated by using (2) or (3):

$$\alpha = 2 \times \arccos\left(\left(\frac{1}{\cos(\beta/2)}\right) \times \left(1 - \frac{l_2^2}{2l_1^2}\right)\right) \qquad (2)$$

$$\beta = 2 \times \arccos\left(\left(\frac{1}{\cos(\alpha/2)}\right) \times \left(1 - \frac{l_2^2}{2l_1^2}\right)\right) \qquad (3)$$

The unfolded eggbox unit element is shown in Fig. 1(a), the sector angle φ_s can be calculated by using (4):

$$\varphi_s = \arccos\left(\frac{2l_1^2 - l_2^2}{2l_1^2}\right) \qquad (4)$$

The volumetric parameters of an eggbox unit element is shown in Fig. 1(c) where the overall dimensions w, l, and h can be calculated by using (5), (6), and (7), respectively:

$$w = 2l_1 \sin(0.5\beta) \qquad (5)$$

$$l = 2l_1 \sin(0.5\alpha) \qquad (6)$$

$$h = l_1 \cos(0.5\alpha) + l_1 \cos(0.5\beta) \qquad (7)$$

To ensure a good foldability and ease of fabrication, the eggbox configuration in this study is optimized to be $l_1 = 20$ mm, $l_2 = 20$ mm, α(unfolded) = 110°, β(unfolded) = 110°. The variation of different geometric parameters with different folding angles α is
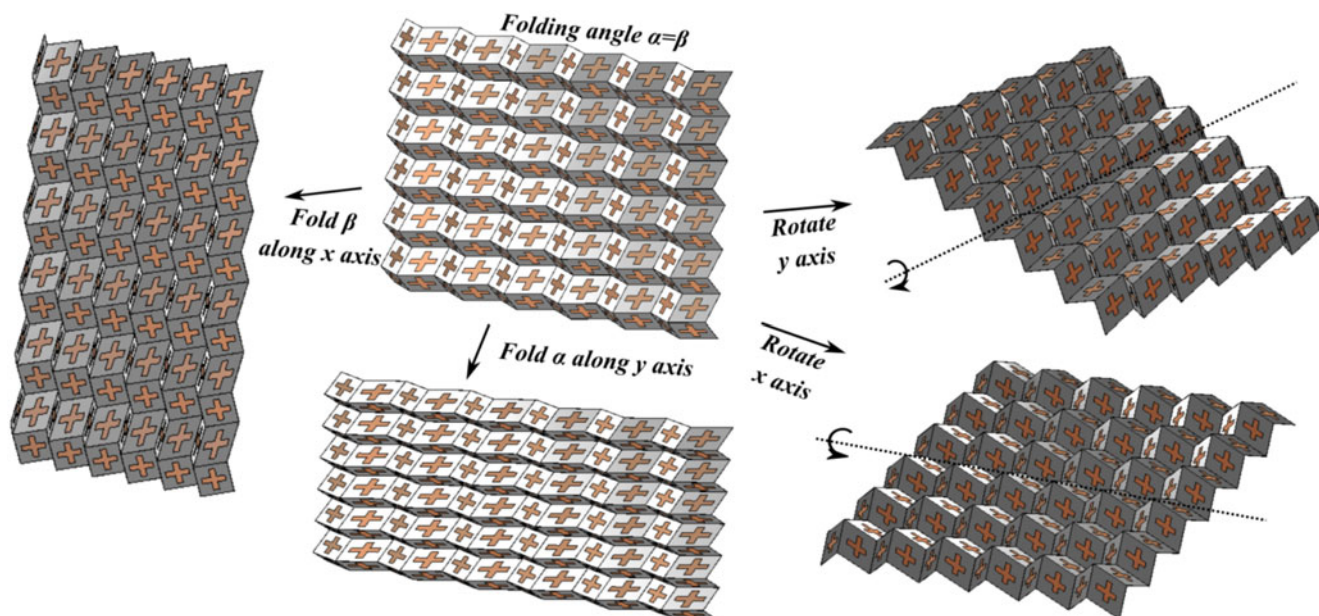
Fig. 4. Demonstration of 4-DOF tuning methodology: fold along *x*-axis; fold along *y*-axis; rotate *x*-axis; and rotate *y*-axis.
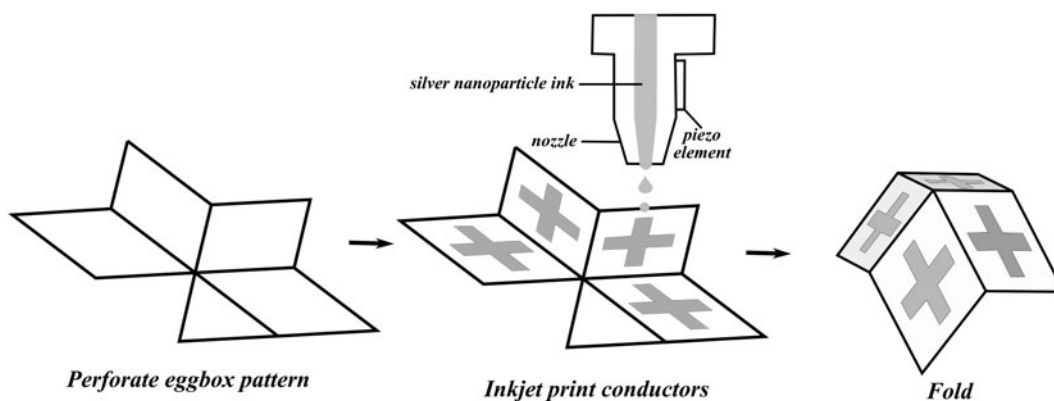

Fig. 5. Three-step fabrication process for eggbox FSS: perforate eggbox pattern; inkjet print conductive traces; and fold to 3D eggbox structure.

shown in Fig. 2 which presents the folding/compressing process of the eggbox structure.

RF design

For proof-of-concept verification, the substrate utilized in this study is 110 µm thick cellulose paper. The material is characterized resulting with a dielectric constant (ε_r) of 3.4 at 7.5 GHz with a loss tangent (tanδ) of 0.015.

To ensure a significant frequency tunability and take full advantage of the eggbox structure with added degrees of freedom, a cross-dipole-shaped conductive pattern is utilized. Cross-dipole FSS element has been well studied over the years showing enhanced bandwidth, dual linear polarizations, and ease of fabrication [1, 21–24]. The authors in [11] explore the possibility of integrating cross-dipole element onto Miura-Ori-based FSS, showing improved tunability and bandwidth.

The eggbox FSS element shown in Fig. 3 is designed and simulated in CST Studio Suite 2019 with unit cell boundary condition and Floquet port excitations with the frequency domain solver.

The unit cell boundary condition simulates only one singular FSS element and extrapolates to an infinite sheet. The size and distribution of the cross-dipole element is optimized to ensure a great range of tunable frequencies and S_{21} performance. The center frequency is designed at 7.5 GHz with optimized cross-dipole dimensions of $l_c = 15$ mm and $w_c = 3.5$ mm. The simulated frequency response will be presented and discussed in Section "6 × 6 Eggbox FSS design" with the measurement results.

6 × 6 Eggbox FSS design

Mechanical simulation

As a proof-of-concept demonstrator, a 6 × 6 "eggbox" FSS with cross-shaped resonating elements is employed in this study. The center frequency is designed at 7.5 GHz. The length of the FSS can be compressed from 170 mm ($\alpha = \beta = \theta_0 = 110°$) down to 37 mm ($\alpha = \beta = 22°$). The AoI can be customized from 0 to 30°. The design takes advantage of the bidirectional symmetry nature of the eggbox structure, tuning both orthogonal polarizations.
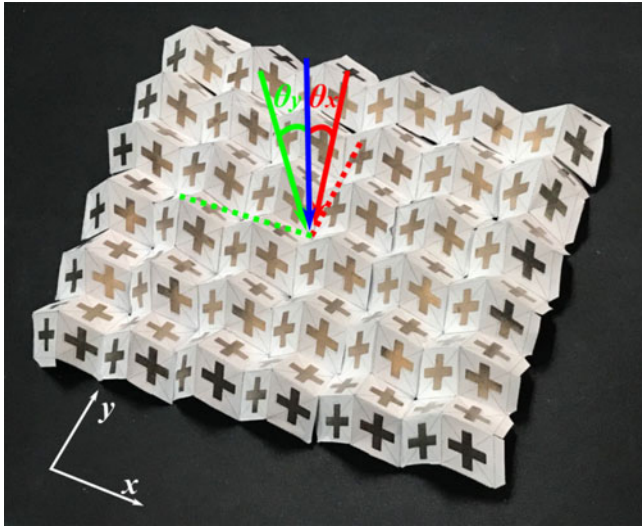
Fig. 6. Fabricated sample of 6 × 6 cross-dipole eggbox FSS and incidence angles: normal incidence (blue), rotate *y*-axis (green), and rotate *x*-axis (red).
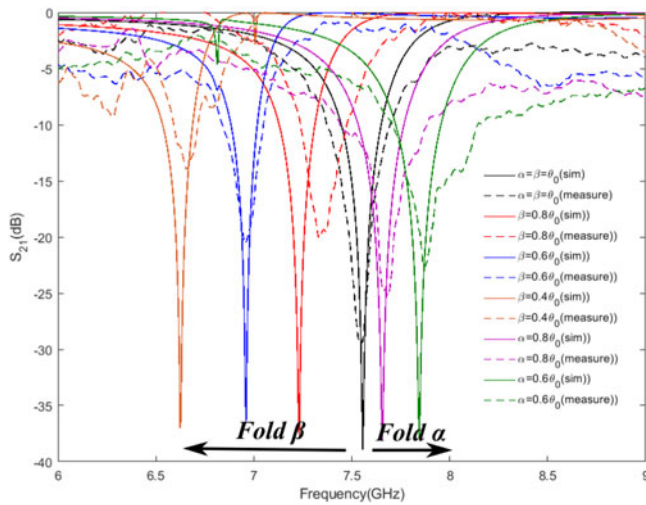

Fig. 8. Vertical (*y*-axis) polarization with different folding angles simulation and measurement results.

Fig. 7. Horizontal (*x*-axis) polarization with different folding angles simulation and measurement results.
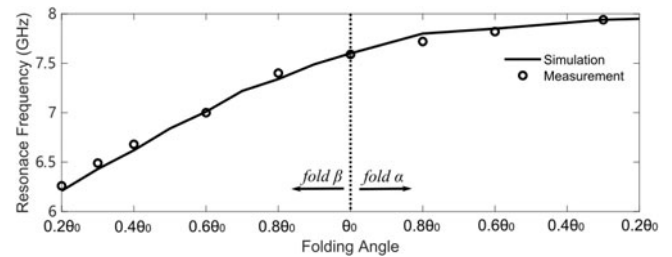
Fig. 9. Resonance frequency versus folding angles of horizontal polarization (*x*-axis).

When compressing along the *x*-axis (as shown in Fig. 4), the decreased equivalent inductance of the horizontally faced branches, increase the resonant frequency of the horizontally polarized waves. The increased equivalent capacitance of the vertically faced branches, decrease the resonant frequency of the vertically polarized waves. Compressing along the *y*-axis will in contrast decrease the horizontally polarized frequency and increase vertically polarized frequency.

When rotating the structure along the *x*-axis, the increased equivalent inductance of the horizontally faced branches, decrease the resonant frequency of the horizontally polarized waves. Rotating along the *y*-axis will in contrast decrease the vertically polarized frequency.

Fabrication

Unlike the Miura structure, the eggbox is a non-developable structure that cannot be folded out of a single planar paper
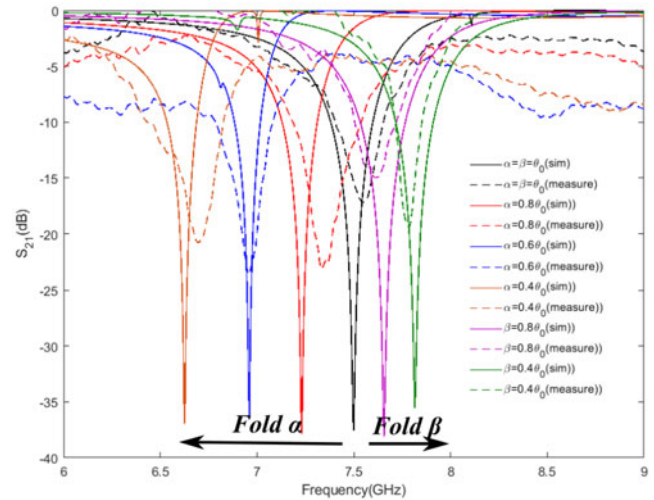
sheet. Therefore, to realize the eggbox with a paper-based substrate, we will utilize cuts and folds of individual eggbox FSS elements which are then adhered together. In this case, the manual fabrication process is durable and accurate enough for this proof-of-concept demonstration. To further improve the fabrication process, the 4D hybrid printing process has been studied in recent years [4, 25]; 4D printing can be a faster and more accurate way to manufacture a scalable and durable eggbox FSS.

The print-fold-attach fabrication process shown in Fig. 5 is utilized to realize the eggbox FSS prototype, which consists of a 6 × 6 array of individual cells. First, a folding pattern for the individual eggbox cell was designed in 2D CAD software. The 2D drawing accounts for the conductive traces, the folds, and an additional polygon to glue the edges that enable linking of the elements together that can be easily printed with an office laserjet printer. Then, the cross-dipole pattern will be printed onto the flat eggbox outline with a Dimatix DMP-2831 inkjet printer utilizing Suntronic EMD5730 silver nanoparticle (SNP) ink (Sigma-Aldrich). Cellulose paper inherently tends to absorb the conductive ink, thus, 10 layers of SNP ink is printed to ensure an exceptional conductivity and flexibility. After printing, the substrate will be thermally cured at 140℃ for 1 h to sinter the SNP ink. Finally, to realize the eggbox 6 × 6 matrix, each folded structure was attached together by glue. The entirety of the 6 × 6 matrix of elements is shown in Fig. 6, with an approximate length and width of 170 mm × 170 mm in its uncompressed state.
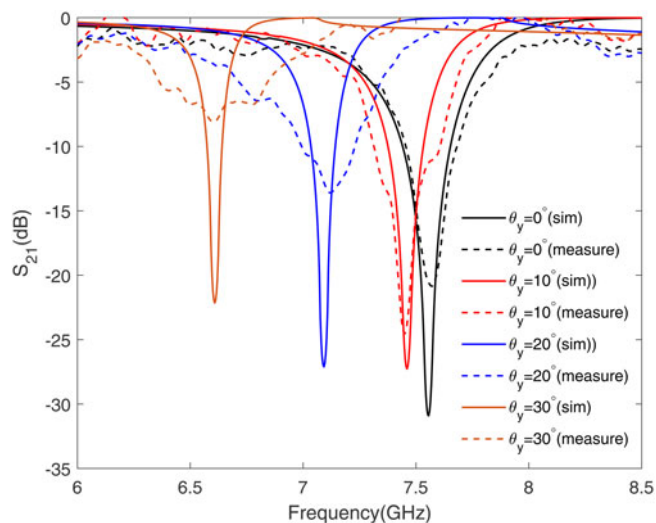
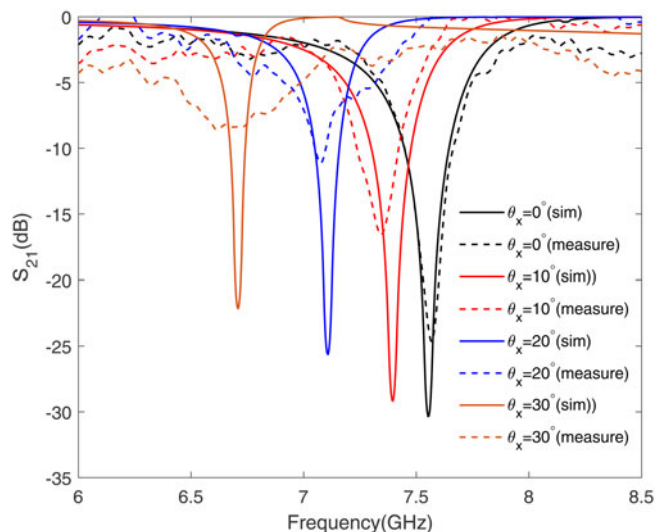Fig. 10. Horizontal polarization (x-axis) with different y-axis rotating angles simulation and measurement results.

Fig. 11. Vertical polarization (y-axis) with different x-axis rotating angles simulation and measurement results.

Simulation and measurement results

In order to measure the fabricated prototype, two horn antennas (A-INFOMW LB-20245-SF) were placed equidistant with 1.5 m spacing, with the results measured on an Anritsu MS46522B VNA set to measure from 6 to 9 GHz. The 6×6 eggbox structure is placed equidistant between the horn antennas. The eggbox structure was compressed for different angles α and β, and the length and width of the eggbox after various compressions enables determination of the fold angles α and β, which are then compared to the simulated results.

The simulated and measured insertion loss of the eggbox FSS for horizontal polarization (along the x-axis) with different folding angles is shown in Fig. 7. From this figure, the resonant frequency of the metamaterial shifts higher as the folding angle β decreases. This is due to the reduced effective length of the horizontal branch of the cross element due to folding, which in turn causes a reduction of the inductance. On the other hand, the

Table 1. Performance comparison of typical origami-inspired FSS

Study	Type	Pattern	Frequency tunable	
			range (%)	Polarization
[2]	Miura	Dipole	12.8	Linear
[4]	Miura	Dipole	13.5	Linear
[11]	Miura	Cross	19	Dual-linear
This study	Eggbox	Cross	25	Dual-linear, 4-DOF-tunable

resonant frequency of the origami meta-material shifts lower as the folding angle α decreases. The result of this is due to the folding along the y-axis reducing the gap between the horizontal components of the metamaterial, leading to an increased capacitance that reduces the resonant frequency. The vertical polarization response is demonstrated in Fig. 8. In this scenario, as the folding angle of β decreases, the frequency reduces due to the increase of capacitance. If the folding angle α is reduced, the frequency of the resonant response increases due to a reduced inductance. Note that the amount of frequency shifting varies depending on the folding direction and polarization. For example, it can be seen that the folding angle β has an increased impact on the response of the system along the horizontal polarization. Similarly, along the folding angle α has a larger impact of the response in the vertical polarization along the y-axis. The measured resonance frequency versus folding angles ($0.2\theta_0$ to θ_0) of horizontal polarization is shown in Fig. 9, the measured fractional bandwidth is 25%.

The simulated and measured insertion loss of the eggbox FSS for horizontal polarization (along the x-axis) with different y-axis rotating angles θ_y is shown in Fig. 10. The resonant frequency of the eggbox FSS decreases as the rotating angle θ_y increases. This is due to the expanded effective length of the vertical branch of the cross element due to folding, which in turn causes an increase of the inductance. On the other hand, in Fig. 11, the resonant frequency of the horizontal branch shifts lower as the rotating angle θ_x increases.

There are some mismatches between the simulation and measurement results especially the amplitude of the insertion loss. This is because the simulation setup uses unit cell boundary condition in CST, which considers the FSS as infinitely large. The unfolded 6×6 eggbox FSS (170 mm $\times$ 170 mm) will cover the whole antenna aperture which can be considered as infinity large. However, when we compress or rotate the structure, the size of the eggbox FSS can reduce to 37 mm $\times$ 170 mm which cannot cover the entire illuminating antenna beamwidth anymore, causing leakage that reduces the insertion loss performance.

The measured performance of the eggbox FSS design presented in this paper is compared with state-of-the-art origami FSSs and the result is shown in Table 1. The proposed design demonstrates widest tunable range, dual linear polarizations, and 4-DOF tunability.

Conclusion

This paper demonstrated a novel tunable eggbox-based origami 3D FSS. The eggbox structure enables two foldable directions

and two rotatable axes to tune the resonant frequency. The measured results show a wide range of frequency control of 25% fractional bandwidth. The fabrication of individual cells without the use of active devices enables easy scalability by allowing many individual elements to be fabricated and then assembled in any desired configuration. By changing the type of substrate [26], or fabricate with 3D printing technology [4], the design can be applicable for remote sensing, RFID, 5G, and mm-wave applications.

References

1. **Munk BA** (2000) *Frequency Selective Surfaces: Theory and Design*, New York: John Wiley & Sons.
2. **Nauroze SA, *et al.*** (2018) Continuous-range tunable multilayer frequency-selective surfaces using origami and inkjet printing. *National Academy of Sciences* **115**, 13210–13215.
3. **Mologni JF, *et al.*** (2017) Investigation on the deployment of FSS as electromagnetic shielding for 5G devices, 2017 SBMO/IEEE MTT-S International Microwave and Optoelectronics Conference (IMOC), Aguas de Lindoia.
4. **Cui Y, *et al.*** (2019) Novel 3D-Printed Reconfigurable Origami Frequency Selective Surfaces With Flexible Inkjet-Printed Conductor Traces, 2019 IEEE MTT-S International Microwave Symposium (IMS), Boston, MA, USA.
5. **Costa F, *et al.*** (2012) A frequency selective radome with wideband absorbing properties. *IEEE Transactions on Antennas and Propagation* **60**, 2740–2747.
6. **Jeong H, *et al.*** (2020) Hybrid (3D and inkjet) printed electromagnetic pressure sensor using metamaterial absorber. *Additive Manufacturing* **35**, 101405.
7. **Ibrahim SH, *et al.*** (2019) Tunable FSS Using PIN Diodes and Microcontroller, 2019 IEEE Jordan International Joint Conference on Electrical Engineering and Information Technology (JEEIT), Amman, Jordan.
8. **Rahmani-Shams Y, *et al.*** (2018) Dual band low profile and compact tunable frequency selective surface with wide tuning range. *Journal of Applied Physics* **123**, 235301.
9. **Sazegar M, *et al.*** (2012) Beam steering transmitarray using tunable frequency selective surface with integrated ferroelectric varactors. *IEEE Transactions on Antennas and Propagation* **60**, 5690–5699.
10. **Schoenlinner B, *et al.*** (2004) Switchable RF MEMS Ka-band frequency-selective surface, 2004 IEEE MTT-S International Microwave Symposium Digest (IEEE Cat. No. 04CH37535), Fort Worth, TX, USA.
11. **Fuchi K, *et al.*** (2012) Origami tunable frequency selective surfaces. *IEEE Antennas and Wireless Propagation Letters* **11**, 473–475.
12. **Biswas A, *et al.*** (2019) A Dual-Band Origami FSS, 2019 IEEE International Symposium on Antennas and Propagation and USNC-URSI Radio Science Meeting, Atlanta, GA, USA.
13. **Deanna S, *et al.*** (2019) Origami-inspired frequency selective surface with fixed frequency response under folding. *Sensors* (Basel, Switzerland) **19**, 4808.
14. **Biswas A, *et al.*** (2020) Transforming single-band static FSS to dual-band dynamic FSS using origami. *Scientific Reports* **10**, 13884.
15. **Schenk M, *et al.*** (2013) Geometry of Miura-folded metamaterials. *National Academy of Sciences* **110**, 3276–3281.
16. **Sareh P, *et al.*** (2015) A framework for the symmetric generalisation of the Miura-ori. *International Journal of Space Structures* **30**, 141–152.
17. **Cui Y, *et al.*** (2021) A Novel Fully Inkjet Printed Dual-Polarization Broadband Tuneable FSS Using Origami "Eggbox" Structure, 2020 50th European Microwave Conference (EuMC), Utrecht, Netherlands, pp. 760–763.
18. **Pratapa P, *et al.*** (2019) Geometric mechanics of origami patterns exhibiting Poisson's ratio switch by breaking mountain and valley assignment. *Physical Review Letters* **122**, 155501.
19. **Xie R, *et al.*** (2015) Parametrisation and application of cube and eggbox-type folded geometries. *International Journal of Space Structures* **30**, 99–110.
20. **Nassar H, *et al.*** (2016) Curvature, metric and parametrization of origami tessellations: theory and application to the eggbox pattern. *Proceedings of the Royal Society A* **473**, 20160705.
21. **Kiani GI, *et al.*** (2011) Cross-dipole bandpass frequency selective surface for energy-saving glass used in buildings. *IEEE Transactions on Antennas and Propagation* **59**, 520–525.
22. **Seman FC, *et al.*** (2018) Phase Characteristics of Multi-Layer Crossed-dipole FSS in Salisbury Screen Absorber, 2018 IEEE International RF and Microwave Conference (RFM), Penang, Malaysia.
23. **Majumdar P, *et al.*** (2018) Equivalent circuit model of cross and circular ring FSS using vector fitting, 2018 IEEE Proceedings of 2014 3rd Asia-Pacific Conference on Antennas and Propagation, Harbin.
24. **Zouaoui Y, *et al.*** (2019) Cross Dipole FSS Bandwidth Enhancement, 2019 IEEE International Symposium on Antennas and Propagation and USNC-URSI Radio Science Meeting, Atlanta, GA, USA.
25. **Eid A, *et al.*** (2020) Inkjet-/3D-/4D-printed perpetual electronics and modules: RF and mm-wave devices for 5G+, IoT, smart agriculture, and smart cities applications. *IEEE Microwave Magazine* **21**, 87–103.
26. **Nauroze SA, *et al.*** (2019) A thermally actuated fully inkjet-printed origami-inspired multilayer frequency selective surface with continuous-range tunability using polyester-based substrates. *IEEE Transactions on Microwave Theory and Techniques* **67**, 4944–4954.
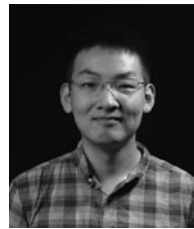
Yepu Cui received his B.S. degree in electrical engineering from the Harbin Institute of Technology, Harbin, China, in 2017. He is currently pursuing his Ph.D. degree with the School of Electrical and Computer Engineering, Georgia Institute of Technology, Atlanta, GA, USA. He is a member of the ATHENA Research Group. His research focuses on the design and fabrication of mm-wave conformal arrays and antennas, origami-inspired tunable frequency selective surfaces, chipless RFID sensors, and other high-performance microwave devices. He develops additive hybrid printing manufacturing processes combining 3D printing technologies with inkjet printing technologies to realize complex RF structures.

Ryan A. Bahr received his B.S. degree (summa cum laude) with a focus on RF engineering and his M.S. degree with a focus on electromagnetics and a minor in computer science from the Georgia Institute of Technology, Atlanta, GA, USA, in 2013 and 2015, respectively. He is currently a Research Assistant with the ATHENA Research Laboratory, Georgia Institute of Technology, where he focuses on the development of 3D electromagnetic designs utilizing additive manufacturing. He designs complex electromagnetic structures with additive manufacturing utilizing technologies, such as fused deposition modeling, stereolithography, and inkjet printing. He is involved in mathematically inspired structures, inkjet printing of flexible electronics, and the utilization of additive manufacturing for RF packaging and millimeter-wave electronics.

Samantha V. Rijs is an Electrical Engineering undergraduate from the Georgia Institute of Technology. She joined the ATHENA lab in 2019 to pursue her technical interests. Her main research is on additive manufactured electronic devices such as 3D-printed origami antennas and inkjet-printed circuits on flexible substrates.

Manos M. Tentzeris received his Diploma degree (magna cum laude) in electrical and computer engineering from the National Technical University of Athens, Athens, Greece, and his M.S. and Ph.D. degrees in electrical engineering and computer science from the University of Michigan, Ann Arbor, MI, USA. He was a Visiting Professor with the Technical University of Munich, Munich, Germany, in 2002, a Visiting Professor with GTRI-Ireland, Athlone, Ireland, in 2009, and a Visiting Professor with LAAS-CNRS, Toulouse, France, in 2010. He heads the Agile Technologies for High-Performance Electromagnetic Novel Applications Research Group (20 researchers), Georgia Institute of Technology, Atlanta, GA, USA. He has served as the Head of the GT-ECE Electromagnetics Technical Interest Group, the Georgia Electronic Design Center Associate Director of the RFID/Sensors Research, the Georgia Tech NSF-Packaging Research Center Associate Director of the RF Research, and the RF Alliance Leader. He is currently a Ken Byers Professor of flexible electronics with the School of Electrical and Computer Engineering, Georgia Institute of Technology. He has authored over 650 papers in refereed journals and conference proceedings, five books, and 25 book chapters. He holds 14 patents. He has given over 100 invited talks to various universities and companies all over the world. He has helped develop academic programs in 3-D-/inkjet-printed RF electronics and modules, flexible electronics, origami and morphing electromagnetics, highly integrated/multilayer packaging for RF and wireless applications using ceramic and organic flexible materials, paper-based RFIDs and sensors, wireless sensors and biosensors, wearable electronics, green electronics, energy harvesting and wireless power transfer, nanotechnology applications in RF, microwave MEMS, and SOP-integrated (ultra-wideband, multiband, mmW, and conformal) antennas.